Received: 13 August 2024 | Revised: 29 September 2024 | Accepted: 4 October 2024

DOI: 10.1002/fam.3246

RESEARCH ARTICLE

WILEY

The emission of pollutants from ornamental shrubs during forest fires

Bruno Martinent | Camille Luciani | Virginie Tihay-Felicelli | Franck Renucci | Paul-Antoine Santoni | Toussaint Barboni

University of Corsica—CNRS UMR 6134 SPE, Corte, France

Correspondence
Toussaint Barboni, University of Corsica—CNRS UMR 6134 SPE, Campus Grimaldi, BP 52, 20250 Corte, France.
Email: barboni@univ-corse.fr

Abstract

This study investigates the combustion behavior, emissions, and aerosol production of four plant species: *Laurus nobilis*, *Cistus monspeliensis*, *Photinia fraseri*, and *Cupressus sempervirens*. The Heat Release Rate (HRR) and Smoke Production Rate (SPR) were measured, revealing that *Cupressus sempervirens* had the highest HRR and longest flame duration due to its higher bulk density. Emission Factors (EFs) for key compounds such as CO_2, CO, NO, and aerosols showed significant variation by species. Aerosol analysis indicated that the combustion of all plants primarily emitted fine particles, with the majority being ultrafine particles ($PM_{0.1}$), particularly in the 25–130-nm range. Particle size distributions were bimodal in number but monomodal in volume. These findings highlight the impact of plant characteristics on fire behavior and emissions, with significant implications for understanding fire dynamics in wildland–urban interfaces.

KEYWORDS
Aerosols, Elpi +, Heat Release Rate, Smoke, Smoke production Rate (SPR)

1 | INTRODUCTION

Wildfires are both natural and human-caused events that have significant impacts on ecosystems, human health, and the environment. These fires can, on the one hand, destroy infrastructure and lead to fatalities. In recent years, as a result of global warming, the hot and dry seasons are getting longer, and forest fires are becoming more intense and destructive. Major fires in Canada, California, Australia, Greece, and Gironde have forced the evacuation of large numbers of people, destroyed thousands of structures, and resulted in increasingly high insurance costs. Even more tragically, they cost the lives of many local residents.[1–6] As well as climatic conditions that favor the ignition and spread of fires, these regions are also characterized by areas where wild or ornamental vegetation mixes with human habitation, forming what are known as wildland–urban interfaces (WUIs). There are different types of WUI, such as linear areas, where natural forest vegetation, ornamental vegetation, and human infrastructure are separated by a line, and intermingled areas, where vegetation and human structures are completely intertwined.[6,7] In the current context of climate change and demographic expansion, WUIs are an emerging issue in fire safety science. In addition, human pressure on forests continues to increase, leading to an increased risk of property destruction and injury.[8] Forest fires in the WUI are particularly critical situations, as they present a high risk to human life and property due to the proximity of inhabited areas to wooded areas.[2,3]

As well as being destructive, forest fires emit large quantities of smoke, which is known to be toxic and can cause death. Recent tragic fires in southern Europe illustrate this reality, with 115 deaths in Portugal in 2017 and 102 deaths in Greece in 2018.[6] During these fires, residents and firefighters were trapped, exposed to large

This is an open access article under the terms of the Creative Commons Attribution License, which permits use, distribution and reproduction in any medium, provided the original work is properly cited.
© 2024 The Author(s). *Fire and Materials* published by John Wiley & Sons Ltd.

quantities of smoke and suffocated, leading to deaths in their homes and on the roads.[4,6] Wildfires release a range of air pollutants, such as fine and ultrafine particles, volatile organic compounds (VOC), and semi-volatile organic compounds (SVOC), including aldehydes, polycyclic aromatic hydrocarbons (PAH), and other organic and inorganic compounds, as well as nitrogen oxides (NOx), carbon monoxide (CO), and carbon dioxide (CO_2).[9–17] Smoke aerosols are heterogenously distributed among different size of particles. Through the analysis of their composition and morphology, distinct types of aerosols have been identified, including soot, tars, and organic particles containing inorganic inclusions predominantly composed of potassium, chlorides, and sulfates called ashes. These findings are based on emissions from savanna and forest fires.[18,19] These studies demonstrate that the particles emitted by these fires exhibit a wide range of shapes and compositions, highlighting the complexity of combustion processes and chemical interactions in these natural environments. Inhaling smoke emissions can cause acute and chronic respiratory problems, as well as irritations of the eyes, throat, and respiratory tract. It can also lead to neurological, cardiovascular, and microvascular health effects.[20–22] Fine particles, especially, can penetrate deeply into the respiratory tract and cause or worsen respiratory, cardiovascular, and neurological problems.[20] Inhalation of wildfire smoke can result in increased hospitalizations for respiratory problems, asthma exacerbations, eye and throat irritations, headaches, dizziness, and other symptoms. The most vulnerable populations, such as children, the elderly, and those with preexisting cardiorespiratory diseases, are particularly at risk.[20] Emissions from biomass burning depend mainly on the fuel composition, fuel moisture content, fuel load, fire intensity and combustion type.[23,24]

It is important to characterize the smoke emitted in WUIs because the pollutants it contains can vary depending on the type of fuel, whether it is forest vegetation or ornamental plants. This smoke can also enter homes and is often responsible for fatalities in wildland fires. An effective strategy for preventing fires in the wildland–urban interface is to manage vegetation around buildings by creating horizontal and vertical fuel breaks, which help reduce fire intensity and spread. However, post-fire studies have shown that the presence of ornamental trees and hedgerows in residential areas can actually facilitate the spread of fire towards buildings.[3] In order to develop effective methods for reducing fire risk in WUIs, it is important to better understand how different types of vegetation burn, and how the resulting smoke affects human health. The emission of air pollutants from fires in these areas poses significant challenges to both human health and air quality, affecting not only emergency responders but also the populations living in these vulnerable zones.

This paper presents the findings of an experimental study investigating the composition of smoke emitted during the combustion of plant fuels. The influence of four plants was examined: one native to the Mediterranean, and three ornamental species commonly found in WUI. The plants examined were *Cistus monspeliensis*, *Laurus nobilis*, *Photinia fraseri*, and *Cupressus sempervirens*. The aim of this study was to observe the smoke emitted and the fire behavior of these plants when exposed to a fire front spreading over a bed of wood wool on a laboratory scale. The plants were ignited using a Large-Scale Heat Release (LSHR) apparatus. This ignition method was selected to simulate a fire that originated from an underlying layer of burning herbaceous vegetation, which has the highest probability and frequency of occurrence in the defensible zone due to fuel management practices. The mass loss and heat release rate (HRR) of the burning vegetation were quantified. The smoke was analyzed using a Fourier Transform Infrared Spectrometer (FTIR) and an Electrical Low-Pressure Impactor (ELPI+). This article presents the experimental procedure employed in this study, followed by a discussion of the results.

2 | MATERIALS AND METHODS

2.1 | Experimental procedure

Twenty burning experiments were carried out in this experimental campaign, five for each species of plants. The experiments were conducted under a 1 MW LSHR apparatus with a 3 m × 3 m hood and a 1 $m^3 \cdot s^{-1}$ extraction system coupled to an Antaris IGS FTIR Spectrometer (ThermoFisher Scientific) and an ELPI+ (Addair) (Figure 1). Four plant species commonly found in WUI in the Mediterranean were selected: *Cistus monspeliensis*, *Laurus nobilis*, *Photinia fraseri*, and *Cupressus sempervirens*. *Cistus monspeliensis* is a native plant that is abundant in shrubland. *Laurus nobilis*, *Photinia fraseri*, and *Cupressus sempervirens* are commonly used as hedges in WUI. Before experiments, the plants were air-dried in the laboratory with an ambient temperature of 20.3 (±3.5°C) and a relative humidity of 37.9 (±5.8%) to reach a foliar moisture content of 20 (±2%). The branches were placed on a 2 m × 2 m combustion bed in a welded mesh cage measuring 0.5 × 0.5 × 1 m^3. To keep a fuel load representative of those found in nature, the initial mass of plants used for the experiments varied depending on the species considered: 2.46 (±0.05 kg) for *Cistus monspeliensis*, 1.21 (±0.02 kg) for *Laurus nobilis*, 1.16 (±0.07 kg) for *Photinia fraseri*, and 5.01 (±0.01 kg) for *Cupressus sempervirens*. To mimic the ignition of the plants by a flame front spreading across an herbaceous layer, a bed of wood wool made of white pine was positioned in front of the plants. The wood wool was oven-dried at 60°C for 24 hours and sprayed as evenly as possible to make a fuel bed of 0.7 m long (including 0.2 m under the plant) and 0.6 m wide with a thickness of 0.1 m. This resulted in a fuel load of 0.6 kg · m^{-2}. The wood wool bed was ignited with 10 mL of ethanol spread across the width of the bed leading edge. Table 1 shows the elemental analysis, the ash content obtained by calcination at 815°C (ISO 1171 standard) and the low heating value (LHV) measured according to NF EN 15400 standard for the five fuels. The exhaust gases were analyzed for composition, temperature, optical obscuration, and flow speed (measured with a bidirectional probe).

2.2 | Calorimetric calculation

The HRR was measured with the LSHR apparatus by oxygen consumption calorimetry for each test (Equations 1–4). The HRR is given by the following equation[25]:

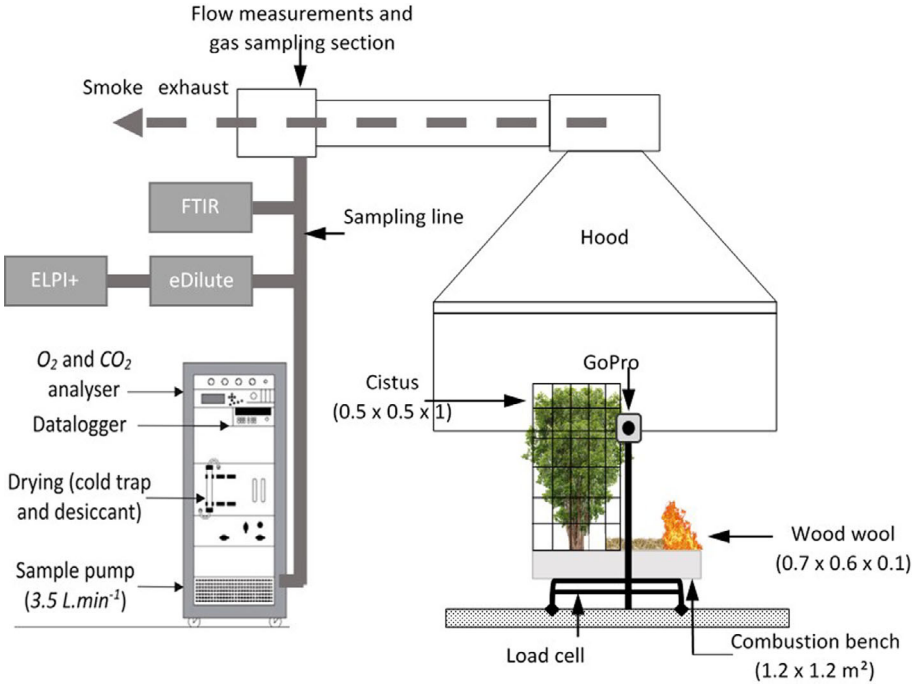


FIGURE 1 Experimental device for the fuel burning. ELPI+, Electrical Low-Pressure Impactor; FTIR, Fourier Transform Infrared Spectrometer.

TABLE 1 Elemental analysis, ash content, and low heating value of the wood wool, *Cistus monspeliensis*, *Laurus nobilis*, *Photinia fraseri*, *and Cupressus sempervirens*.

Fuel	C (%)	H (%)	N (%)	O (%)	Ash (%)	LHV (MJ/kg)	Bulk density (kg · m^{-3})
Wood wool	51.4	6.21	0.24	41.7	0.5	18.966	-
Cistus monspeliensis	50.6	5.9	0.75	38.7	0.7	18.452	8
Laurus nobilis	49.4	6.47	1.51	33.0	8.8	19.322	4
Photinia fraseri	50.5	6.28	0.91	36.9	4.3	19.272	4
Cupressus sempervirens	49.1	6.26	0.92	33.4	8.8	18.045	13

Abbreviation: LHV, low heating value.

$$\mathrm{HRR} = E_{O_2}\left(\dot{n}^0_{O_2} - \dot{n}_{O_2}\right)W_{O_2} \tag{1}$$

where E_{O_2} is the heat release per unit mass of O_2 consumed, $\dot{n}^0_{O_2}$ and $\dot{n}_{O_2}$ represent respectively the molar flow rates of O_2 in incoming air and in the exhaust duct and W_{O_2} is the molecular weight of oxygen.

As the experiments were carried out in an open system, the flow rate of the incoming air was deduced from the flow rate in the exhaust duct. Finally, the HRR was given by the following three relations[23]:

$$\mathrm{HRR} = \frac{E_{O_2}\rho_0 W_{O_2}}{W_{\mathrm{air}}}\left(1 - X^0_{H_2O}\right)X^{a,0}_{O_2}\dot{V}_{S,298}\left[\frac{\phi}{(1-\phi)+\alpha\phi}\right] \tag{2}$$

$$\dot{V}_{S,298} = 22.4A\frac{k_t}{k_p}\sqrt{\frac{\Delta P}{T_s}} \tag{3}$$

$$\phi = \frac{X^{a,0}_{O_2}\left(1 - X^{a}_{CO_2}\right) - X^{a}_{O_2}\left(1 - X^{a,0}_{CO_2}\right)}{X^{a,0}_{O_2}\left(1 - X^{a}_{CO_2} - X^{a}_{O_2}\right)} \tag{4}$$

Where X denotes the molar fraction, W_{air} and ρ_0 are the molecular weight and the density of dry air at 298 K and 1 atm, respectively. $\dot{V}_{s,298}$ is the standard flow rate in the exhaust duct. $\alpha = 1.105$ is the expansion factor for the fraction of the air that was depleted of its oxygen. The superscript 0 is for the incoming air. A is the cross-sectional area of the duct, k_t is a constant determined by calibration with a propane burner, $k_p = 1.108$ for a bidirectional probe, ΔP is the pressure drop across the bidirectional probe, and T_s is the gas temperature in the duct.

To account for the change in plant species, the heat release per unit mass of O_2 consumed was calculated for each plant. For each test, the contribution of wood wool was subtracted from the HRR

TABLE 2 Global equation of combustion for *Cistus monspeliensis*, *Laurus nobilis*, *Photinia fraseri*, and *Cupressus sempervirens*.

Fuels	x	y	z	E_{O_2} (kJ · g^{-1})
Cistus monspeliensis	4.22	5.83	2.51	13.23
Laurus nobilis	4.11	6.41	2.06	12.89
Photinia fraseri	4.21	6.22	2.31	13.07
Cupressus sempervirens	4.09	6.20	2.09	12.27

curves to focus only on the burning of plants. Therefore, based on the ultimate analysis of the species (Table 1), the burning was modeled as follows Equations (5 and 6), with Table 2 for *x*, *y*, and E_{O_2} for each species.

$$C_xH_yO_z + \left(x+\frac{y}{4}-\frac{z}{2}\right)(O_2+3.76N_2) \rightarrow xCO_2+\frac{y}{2}H_2O+3,76\left(x+\frac{y}{4}-\frac{z}{2}\right)N_2 \quad (5)$$

With E_{O_2}

$$E_{O_2}=\frac{\mathrm{LHV}.W_{\mathrm{fuel}}}{n_{O_2}W_{O_2}} \text{ with } n_{O_2}=\left(x+\frac{y}{4}-\frac{z}{2}\right) \quad (6)$$

The sampling rate for HRR was equal to 1 Hz. The variation from the generic value of Huggett's[26] average E_{O_2} (δE_{O_2}) must be taken into account. For example, this variation represents 6.3% for *Cupressus Sempervirens*, and according to Equation (2), such variations will affect the HRR calculations. The variation in HRR due to the variation in E_{O_2} is provided in Santoni et al.,[27] When the composition of the fuel is known, a more accurate value for E_{O_2} can be determined.

2.3 | Chemical analysis of smoke and emission factors

The exhaust gases of combustion were sampled from the exhaust ducts of the LSHR Apparatus and passed through four different analyzers. The first measurement system consists of an Antaris Industrial Gas System (IGS) FTIR-based analyzer from ThermoFisher Scientific. The FTIR spectrometer allows to obtain the molar fractions of CO_2, CO, CH_4, NO, NO_2, NH_3, C_2H_6, C_2H_4, C_2H_2, C_3H_8, C_3H_6, C_4H_6, C_6H_6, HCHO, CH_3CHO, SO_2, H_2O. A filter to remove aerosols was placed before the gas cell and the sampling line was heated at 180°C to avoid condensation. The spectrometer was equipped with a MCT-A detector and a gas cell with a volume of 0.2 L and an optical path-length of 2 m. IR spectra were recorded in the spectral range of 4500 to 550 cm^{-1} with a 0.5 cm^{-1} resolution. The flow rate of the sampling pump was adjusted to 3.5 L · min^{-1}. The identification of the compounds by FTIR was carried out with a database listing the products of combustion. The calibration is checked once a year by a Thermofisher maintenance engineer. The first measurement system consists of non-dispersive infrared (NDIR) spectroscopy. This apparatus was used to quantify continuously CO and CO_2. Each day of analysis, NDIR analysers were calibrated with two points of measurement. The first point corresponds to a gas without CO and CO_2. For this, almost pure N_2 (99.995% i.e., 4.5) was used. For the second point, a mixture containing 2500 ppm of CO and 8% for CO_2 was used. Finally, a double check was made with the CO and CO_2 data recorded with the FTIR. The third analyzer corresponds to the measurement of the extinction of aerosols in the exhaust duct with a He-Ne laser (0.5 mW nominal power) emitting at the red wavelength of 632.8 nm. The length of the optical path in the exhaust duct is 11.4 cm. Finally, an ELPI+ (Dekati) allows to analyze in real-time the particle number size distribution. A particle size distribution is established using the size fractions collected by the impactor stages, with 50% cut-point aerodynamic diameters ranging from 0.0060 µm to 10 µm across stages 1 to 14.[28,29] The airflow velocity of the ELPI+ is maintained at 10 L/min. The operating principle of the ELPI+ involves the precise charging of aerosol particles by a unipolar corona charger, followed by size classification using a low-pressure cascade impactor. Each impactor stage in the series is insulated and connected to sensitive electrometers to measure the electrical current generated by the particle impaction. This electrical current value is directly proportional to the number of particles collected.

The generation of combustion products was quantified in terms of emission factors (EF), EF_i (g · kg^{-1}; Eq. 7), defined as the mass of chemical species *i* produced per dry mass of fuel burned, $m_{b,\mathrm{dry}}$.[16]

$$EF_i=\frac{m_i}{m_{b,dry}} \quad (7)$$

where m_i (kg) is the mass of compound *i* released by the burning and $m_{b,\mathrm{dry}}$ (kg) is the dry mass burned during the experiments. Smoke extinction was measured in the exhaust duct with the He-Ne laser. This allowed to assess the smoke production rate (SPR; Eq. 8) by using the basic smoke equation:

$$\mathrm{SPR}=k\dot{V} \quad (8)$$

where *k* is the light extinction coefficient given by the Bouguer's law and $\dot{V}$ is the standard flow rate in the exhaust duct. Aerosols were also collected on glass fiber filters (37 mm diameter) in the exhaust duct of the LSHR apparatus by using a sample pump (Figure 1). The mass of aerosol (m_a; Eq. 9) released during the burnings was calculated with the following equation:

$$m_a=\int_0^T \frac{k}{\sigma_a}\dot{V}\,dt \quad (9)$$

where σ_a (m^2/kg) is the specific extinction area. The values obtained by[12] for σ_a were used: $\sigma_a = 8290\,\mathrm{m}^2/\mathrm{kg}$. To evaluate the combustion completeness, the modified combustion efficiency (MCE; Eq. 10) was introduced,[16] as follows:

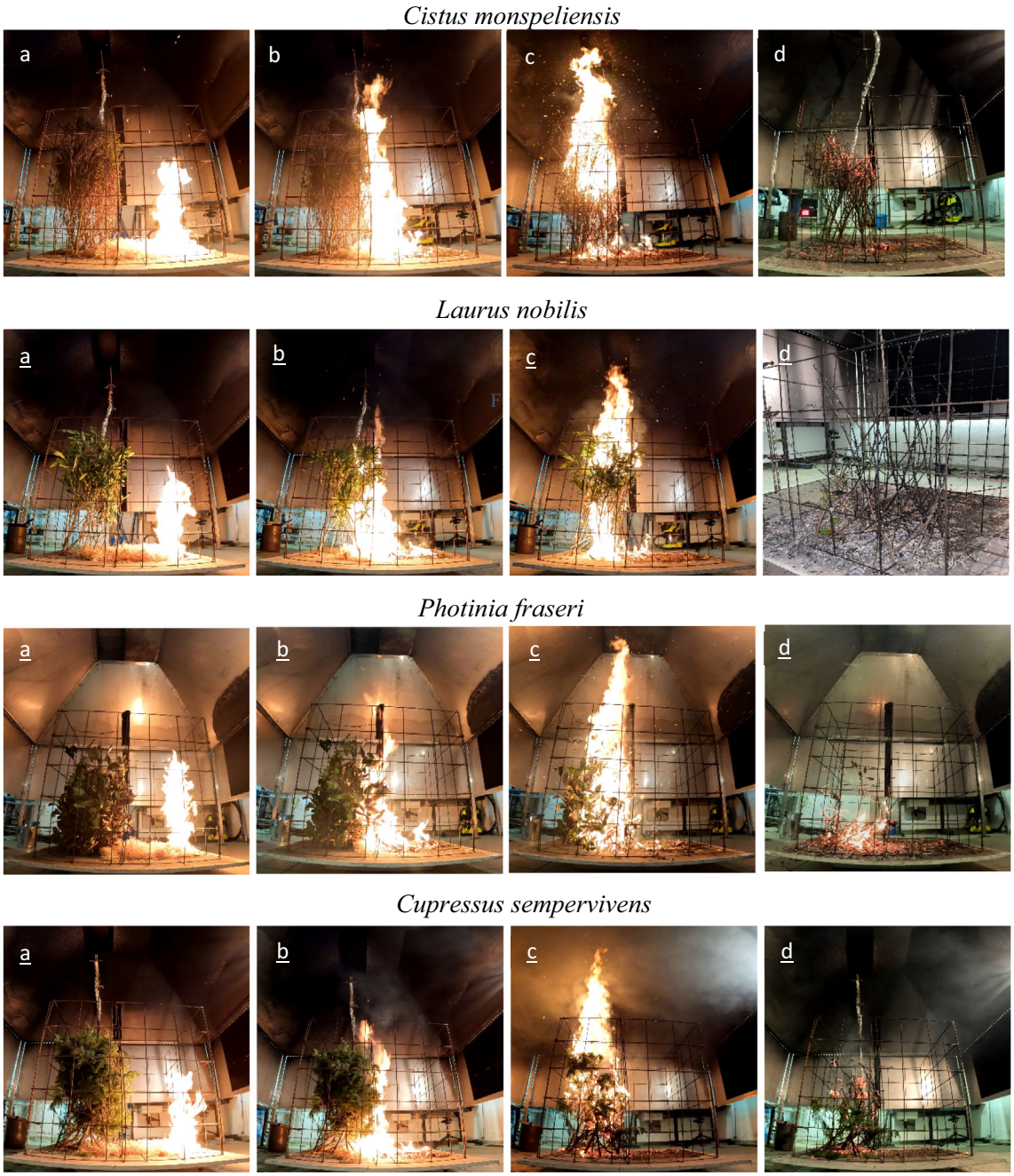


FIGURE 2 Photographs of the plant burning. (A) Fire spread across the wood wool bed; (B) Ignition of the plant; (C) Flame spread within the plant (D) Extinction. (*Cistus monspeliensis*: Ignition of wood wool: $T = 0$ s; Ignition Cistus: $T = 32$ s; PHRR: $T = 55$ s; flame out: $T = 114$ s; *Cupressus sempervivens*: Ignition of wood wool: $T = 0$ s; Ignition Cupressus: $T = 37$ s; PHRR: $T = 65$ s; Flame out: $T = 207$ s; *Laurus nobilis*: Ignition of wood wool: $T = 0$ s; Ignition Laurus: $T = 45$ s; PHRR: $T = 53$ s; Flame out: $T = 86$ s; *Photinia fraseri*: Ignition of wood wool: $T = 0$ s; Ignition Photinia: $T = 39$ s; PHRR: $T = 51$ s; Flame out: $T = 88$ s). HRR, heat release rate. PHRR, peak heat release rate.

$$\mathrm{MCE} = \frac{[\mathrm{CO_2}]}{[\mathrm{CO_2}] + [\mathrm{CO}]} \quad (10)$$

where $[CO_2]$ and $[CO]$ are the molar concentrations of emitted CO_2 and CO in the smoke. Fire-integrated excess molar mixing ratios of CO_2 and CO were used to calculate mean modified combustion efficiencies.

2.4 | Statistical analysis

A multiple-sample comparison test (STATGRAPHICS® Centurion XV) was used. The ANOVA test was chosen to highlight any statistically significant difference between the values measured in all the experiments. If the probability value (p) obtained using the F-test is less than 0.05, there is a difference between the means of the variables with a

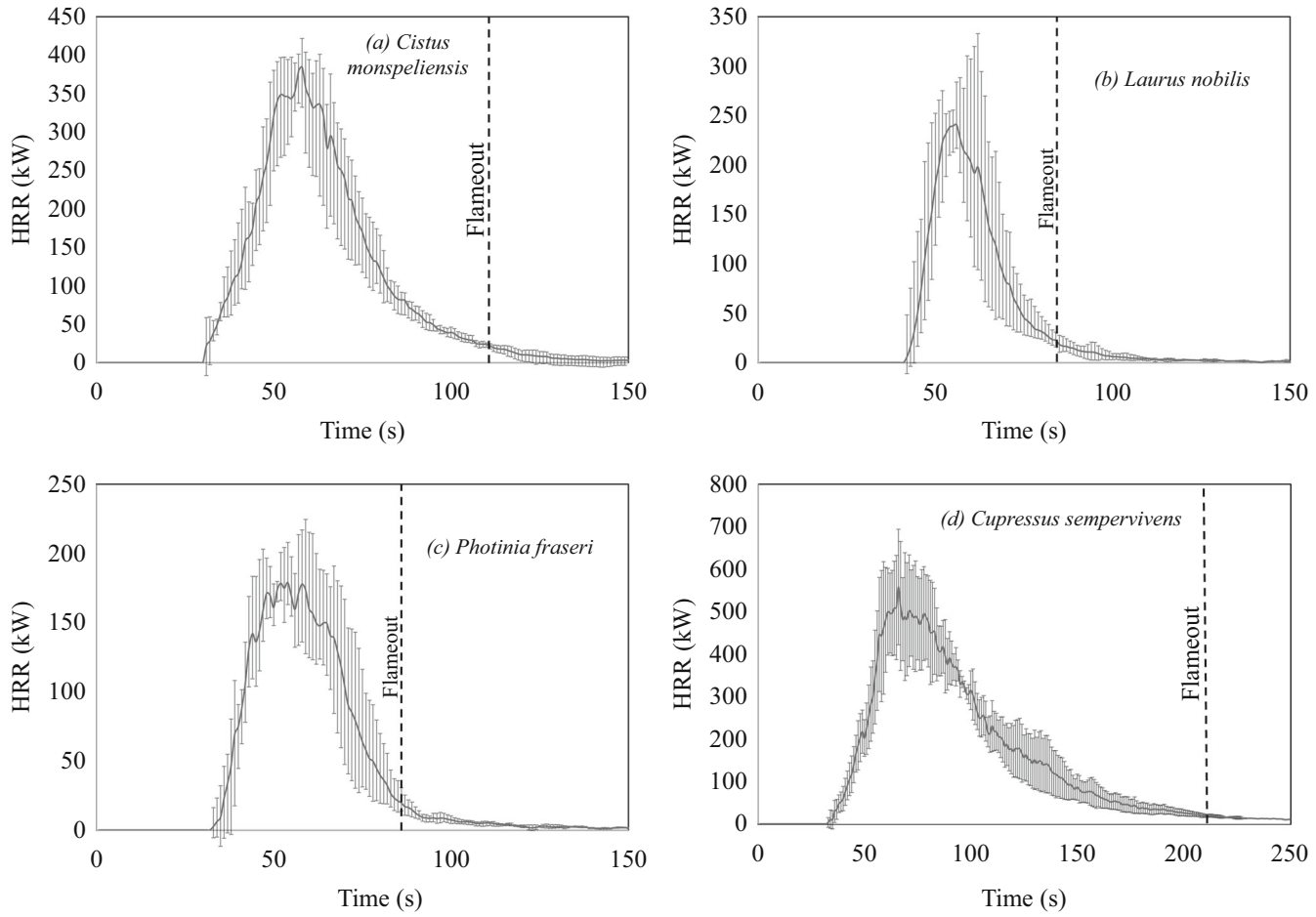


FIGURE 3 Heat release rate over time during the burning of (A) *Cistus monspeliensis*; (B) *Laurus nobilis*; (C) *Photinia fraseri*; and (D) *Cupressus sempervivens*. Error bars corresponds to the difference between the extrema and the average of the replicates.

confidence level of 95%. Multiple-range tests were then used to determine which means were significantly different from each other. The method used to discriminate between the means was Fisher's least significant difference procedure.

3 | RESULTS AND DISCUSSION

3.1 | General description of the burning experiments

The fire tests showed similar behavior for all four plant species (Figure 2). A linear ignition was first performed along the leading edge of the wood wool bed. A flame front quickly established and spread uniformly across the wood wool bed exhibiting a flame height of about 40 cm (Figure 2A). The Ignition of the plant occurred by direct contact of the flame at the base of the crown (Figure 2B). The fire front then spread over the plant (Figure 2C). Then, the decay phase began until the flames were extinguished. After the flameout, only the thicker particles remained (Figure 2D).

The HRRs measured during the experiments for each plant are shown in Figure 3. Since the burning of wood wool was very repeatable, its contribution was subtracted from the HRR curves to focus only on the burning of plants (Figure S1). The vertical bars correspond to the experimental variability observed between the replicates (Figure 3). After plant ignition, the HRR increased rapidly to reach a plateau lasting between 10 and 29 s depending on the species. This phase corresponds to the moment when all branches were on fire. Then, the HRR decreased, corresponding to the decay phase until the flameout followed by the extinction of the residual chars. The peak of the curves and the duration vary depending on the species (Table 3). The highest peak of HRR was observed for *Cupressus sempervirens* (557. 9 kW (±136.9 kW)), followed by *Cistus monspeliensis* (405.8 kW (±11.0 kW)), *Laurus nobilis* (275.8 kW (±29.4 kW)) and *Photinia fraseri* (199.4 kW (±21.2 kW)). The peak measured during the burning of *Cupressus sempervirens* is therefore 2.8 times higher than that of *Photinia fraseri*. The flame duration varies also significantly with the species. The longest combustion was observed for *Cupressus sempervirens* (174 (±9) s), followed by *Cistus monspeliensis* (98 (±10) s), *Photinia fraseri* (49 (±3) s) and *Laurus nobilis* (43 (±3) s). The flame duration for *Cupressus sempervirens* is therefore 2.3 times higher than that of *Laurus nobilis*. Among the four species, *Cupressus sempervirens* is therefore the most combustible plant. This characteristic is due to its bulk density, which is higher than that of the other species

TABLE 3 Peak of heat release rate (HRR) and flame duration measured during the burning.

Species	*Cistus monspeliensis*	*Laurus nobilis*	*Photinia fraseri*	*Cupressus sempervivens*
Peak HRR (kW)	405.8 (±11.0)	275.8 (±29.4)	199.4 (±21.2)	557.9 (±136.9)
Flame duration (s)	98 (±10)	43 (±3)	49 (±3)	174 (±9)

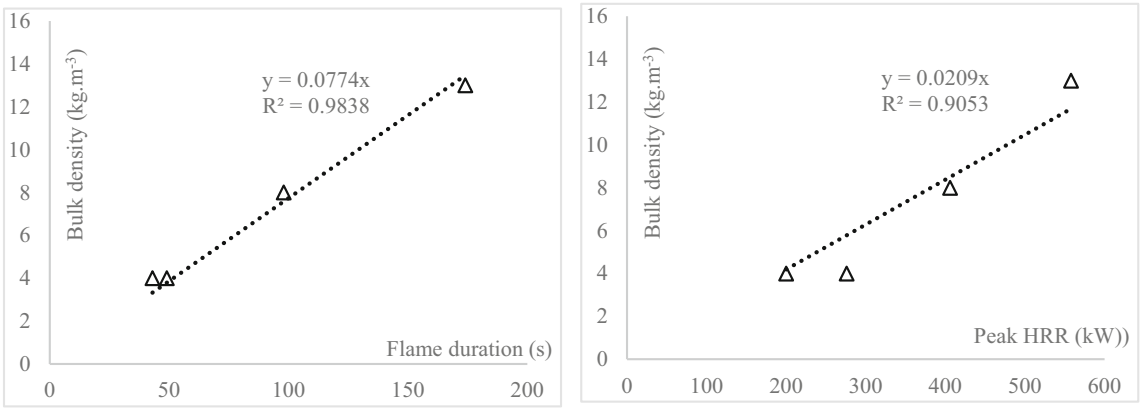


FIGURE 4 Relationship between flame duration and bulk density, and peak HRR and bulk density. HRR, heat release rate.

(13 kg · m^{-3} versus 4 to 8 kg · m^{-3}). This leads to a higher fuel mass for the same plant volume and then to a higher flame duration. This high combustibility of *Cupressus sempervirens* was already observed in previous works[3,30] about ornamental vegetation present in WUI.[31]

Figure 4 shows the relationship between bulk density and flame duration, and peak HRR and bulk density. It can be seen that there is a significant relationship between the bulk density of the plants studied and several combustion parameters, such as flame duration and peak HRR with bulk density. A determination coefficient (R^2) of 0.9967 was found for the relationship between bulk density and flame duration, and 0.9804 between bulk density and peak HRR (Figure 4). It can be seen that the bulk density of the plant is crucial role in the combustion dynamics, influencing both the flame duration and the peak HRR. The higher the bulk density, the longer the flame duration. This is due to the increase in the amount of fuel that allows continuous combustion, thus delaying flame extinction. The bulk density of plants also affects the peak of HRR. A higher density leads to a greater quantity of combustible material present in a given area, resulting in more intense heat release during combustion. It can therefore be concluded that plant bulk density is a determining factor in combustion, directly influencing both flame duration and peak of HRR. These relationships highlight the need for proactive ecosystem management to prevent devastating fires and protect natural habitats.

3.2 | Smoke production

3.2.1 | Smoke production rate

Understanding the pollutants emitted from the combustion of forest fuels is crucial. This knowledge is essential for estimating the potential smoke emissions at forest–human interface areas, particularly during events such as ornamental vegetation fires. By studying these pollutants, we gain valuable insights into the environmental and health impacts of forest fires, as well as the effectiveness of mitigation strategies in protecting both ecosystems and human habitats. Figure 5 illustrates the SPR and HRR during typical fire tests for the burning of the wood wool as well as the spreading of the fire within the plant for the four fuels studied. The burning of wood wool and its smoke production was very repeatable and it was not removed from the SPR curves in Figure 5. In Figure 5, SPR and HRR are the average of the 5 replicates. For all fire tests, the SPR and the HRR follow the same trend during the spreading of the fire the wood wool from until the ignition of the plants (stage 1 in Figure 5). During propagation in wood wool, the mean value of the SPR during this stage is 0.11 (±0.02) $m^2 \cdot s^{-1}$; 0.1 (±0.03) $m^2 \cdot .s^{-1}$; 0.12 (±0.05) $m^2 \cdot s^{-1}$ and 0.14 (±0.02) $m^2 \cdot s^{-1}$ for *Laurus nobilis*, *Cistus monspeliensis*, *Cupressus sempervirens*, and *Photinia fraseri* respectively. After plant ignition, the HRR increased rapidly to reach a plateau lasting between 10 and 29 s depending on the species and the SPR curves follow the HRR curves during combustion in the flaming phase (stage 2 in Figure 5). The mean value of SPR during this stage is 0.15 (±0.07) $m^2 \cdot s^{-1}$; 0.11 (±0.04) $m^2 \cdot s^{-1}$; 0.16 (±0.04) $m^2 \cdot s^{-1}$ and 0.26 (±0.11) $m^2 \cdot s^{-1}$ for *Laurus nobilis*, *Cistus monspeliensis*, *Cupressus sempervirens*, and *Photinia fraseri* respectively. For this stage, the peak SPR for the different fuels are 0.31 (±0.09) $m^2 \cdot s^{-1}$; 0.24 (±0.07) $m^2 \cdot s^{-1}$; 0.28 (±0.09) $m^2 \cdot s^{-1}$ and 0.65 (±0.11) $m^2 \cdot s^{-1}$ for *Laurus nobilis*, *Cistus monspeliensis*, *Cupressus sempervirens*, and *Photinia fraseri* respectively. The observed values are slightly higher than those reported in the literature for the flaming phase of pine needles (mean SPR values: $8.9\times10^{-3} \pm 2\times10^{-4}$ $m^2 \cdot s^{-1}$) or *Cistus monspeliensis* particles (mean SPR values: $9.6\times10^{-3} \pm 1.5\times10^{-3}$ $m^2 \cdot s^{-1}$ for the twigs between 3 and 4 mm).[13,32] There are three reasons for this difference. Firstly, the water content of the material can significantly affect the SPR.

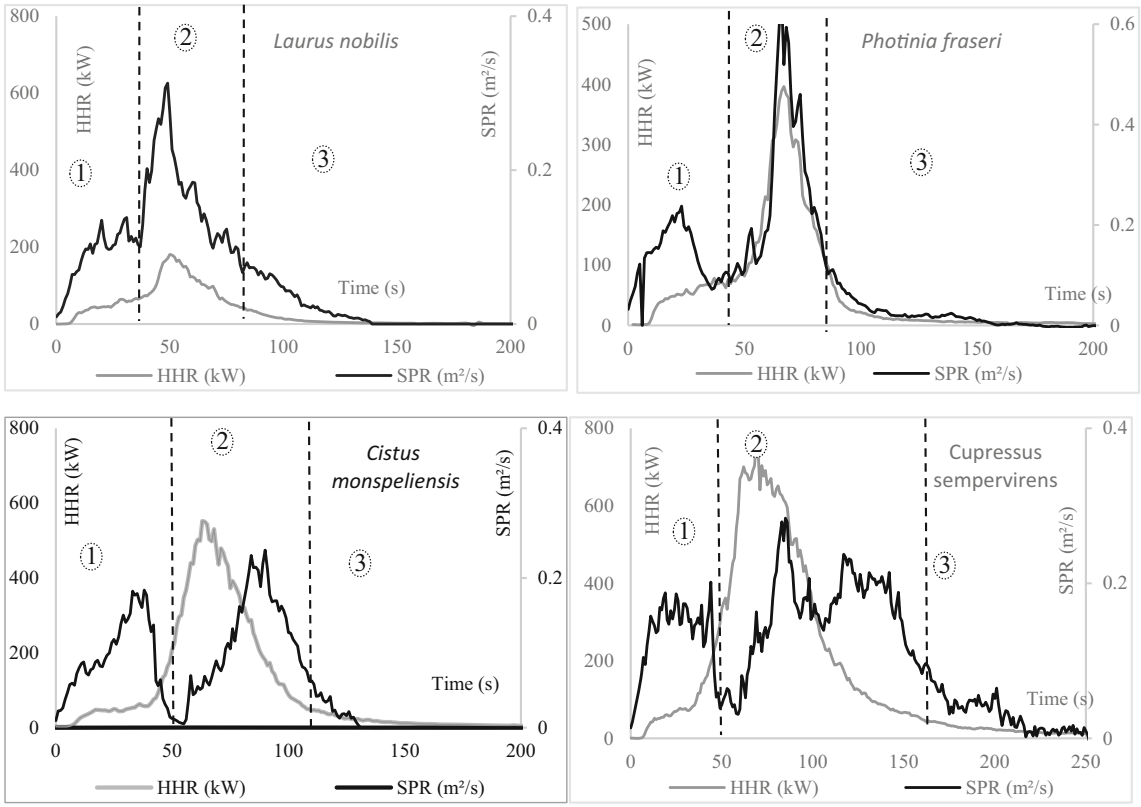


FIGURE 5 The smoke production rate (SPR) and heat release rate (HRR) were measured for the different fuels. The fuels were categorized into three stages: (1) ignition and spreading across the wood wool bed, (2) ignition and combustion of the plant, and (3) smouldering phase.

Second, the amount of oxygen available can affect combustion efficiency and smoke production. Limited oxygen can result in incomplete combustion and higher smoke production and finally, the conditions of the tests are different. Although the experimental conditions involve over-ventilation, some unburned fuel remains after the flameout as well as residual chars. After the flameout (Stage 3 in Figure 5), the glowing of the residual chars occurs as well as the smouldering of remaining twigs. During this last stage, the SPR is 0.03 (±0.03) $m^2 \cdot s^{-1}$; 0.035 (±0.05) $m^2 \cdot s^{-1}$; 0.03 (±0.05) $m^2 \cdot s^{-1}$ and 0.26 (±0.09) $m^2 \cdot s^{-1}$ for *Laurus nobilis*, *Cistus monspeliensis*, *Cupressus sempervirens*, and *Photinia fraseri* respectively. We can thus conclude that the SPR occurs mainly during the flaming stage and for 79%, 85%, 79%, and 82% for *Laurus nobilis*, *Cistus monspeliensis*, *Cupressus sempervirens*, and *Photinia fraseri* respectively with the wood wool was subtracted from the SPR contribution. These results were obtained by integrating the SPR (SPR*time) during the flame phase (stage 2, Figure 5) with respect to the integration of the SPR during the post-flame phase (Stage 3, Figure 5).

3.2.2 | Particle number concentration and size distribution

The properties of aerosols remain poorly understood due to the specific conditions under which they are emitted. These conditions vary not only according to the temperature at which they are formed, but also according to the combustion methods and emission sources. In fact, the particles emitted by forest fires during combustion are composed of different types of material (soot, ashes, unburned material) of different sizes. Therefore, further in-depth studies are required to gain a better understanding of their formation and the quantities emitted during wildfires. Aerosols produced from biomass burning are varied, including soot, tars, fly ash, and coarse fly ash, each emerging at distinct stages during shrub combustion.[33] And, primary aerosol produced by wildland fires is predominantly organic aerosol by mass.[34,35] Figure 6, displays the SPR curves and the particle numbers size distribution obtained with the ELPI+. Despite the potential impact of the nature of the emitted gases and particles on the measurement of opacity, a notable correlation between the SPR curves and the curves of the particle number size distribution is evident. Furthermore, the SPR peak and the size distribution number peak are in alignment. Opacity is a function of particulate concentrations and many other independent optical and physical variables, such as particle size distribution, particle density, refractive index of particles, nature of aerosol (soot, tar, or ash) and gas emitted concentration in the exhaust gas, as examined in previous studies.[36–38] Notwithstanding the aforementioned discrepancy in the detection of the smallest particles, the utilization of He-Ne laser sources facilitates the identification of aerosols with a minimum size of 0.1 μm up to a concentration of 10%. The scattering of light by particles of this size

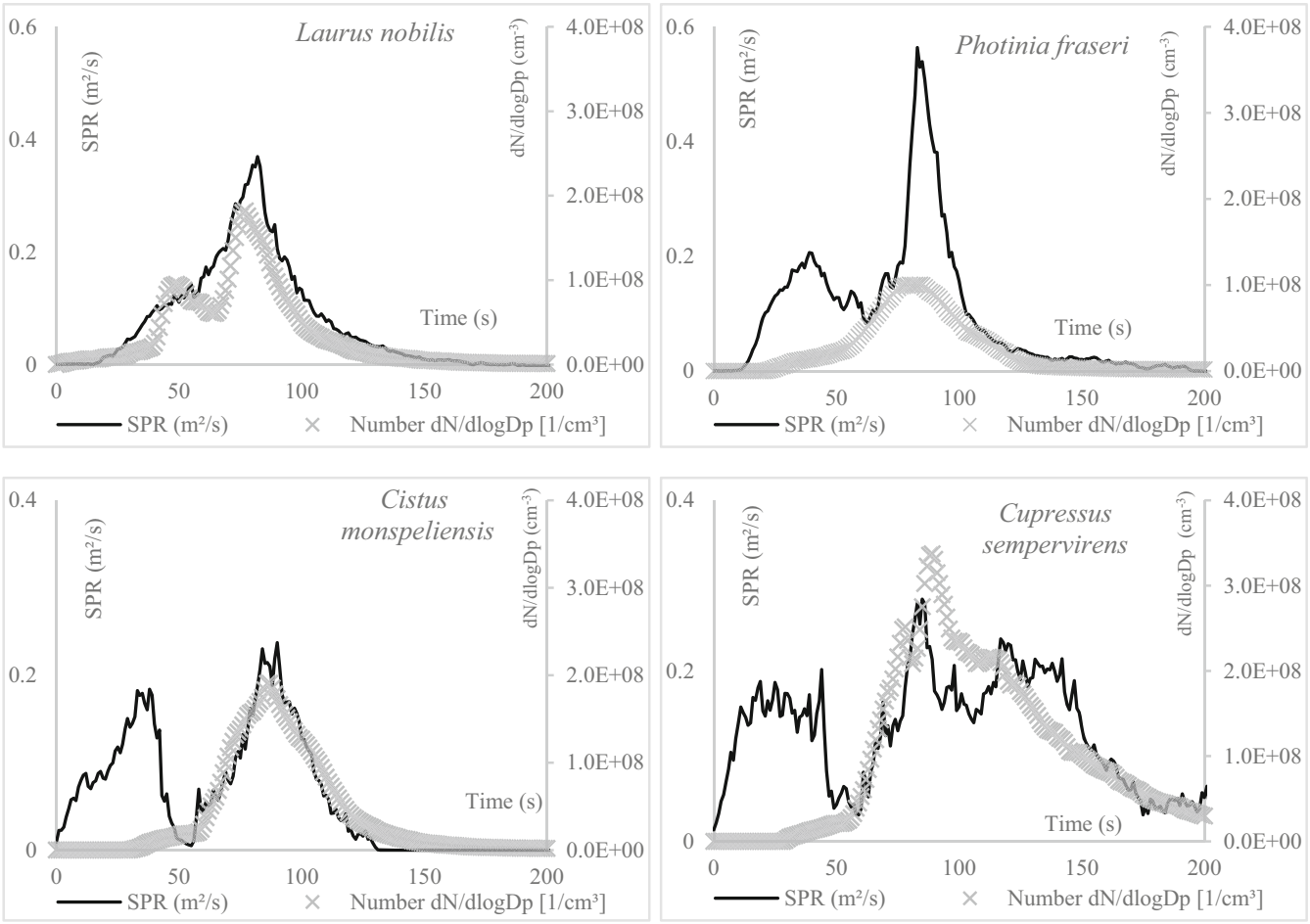
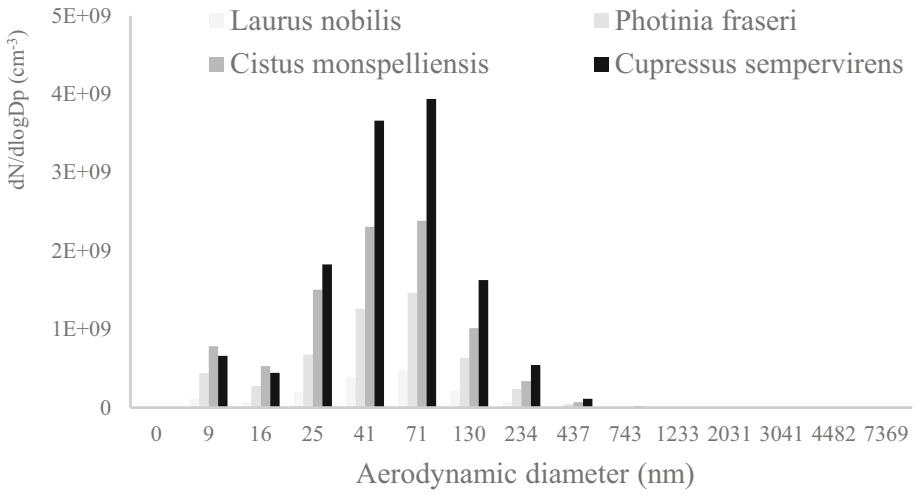


FIGURE 6 Smoke production rate (SPR) and particle number distribution.

FIGURE 7 Particle size distributions in number for all fuels.



allows their concentration and distribution to be determined. More, the principal gases that contribute to high opacity when organic materials are burned include nitrogen oxides (NOx), (CO_2), and (H_2O).

Figure 7 shows the mean of particle number size distributions according to the aerodynamic diameter recorded for the fire tests performed with all plants. The mean of particle number size distribution was calculated using five replicates. We observed that the numerical distribution is centered on the 41–71 nm for all fuels (Figure 7). The mean the sum of particle numbers across all size bins was 1.6×10^9, 5.04×10^9, 8.94×10^9 and 1.28×10^{10} for *Laurus nobilis*, *Cistus monspeliensis*, *Photinia fraseri*, and *Cupressus sempervirens* respectively. We observe that *Cupressus sempervirens* emits the greatest quantity of

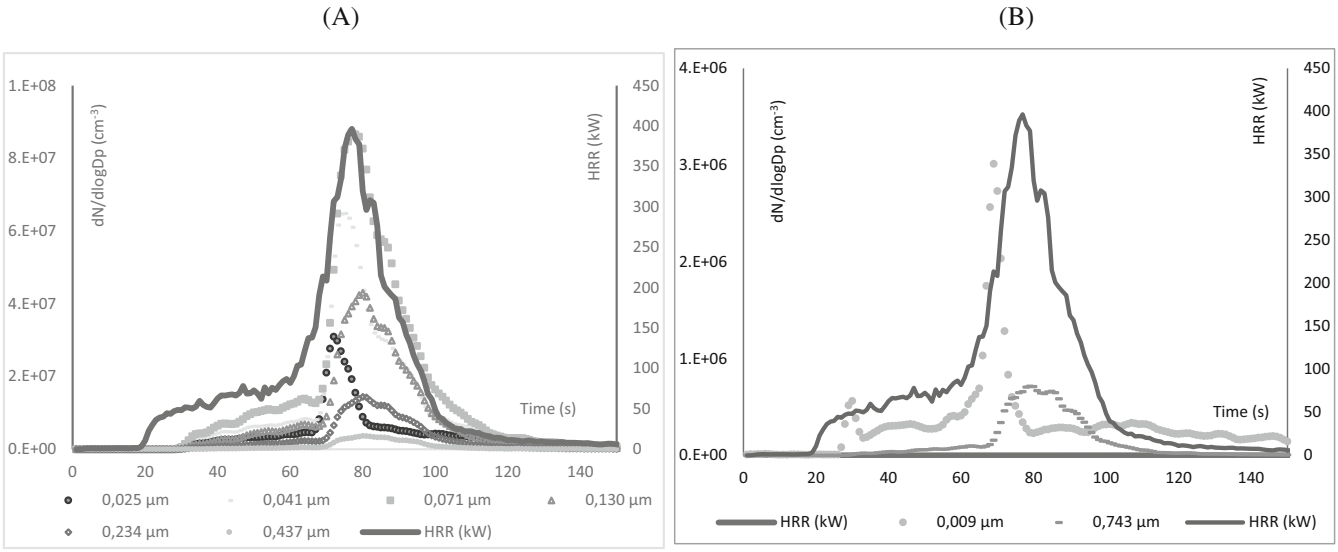


FIGURE 8 Example of particle size distributions in number according to the combustion and the heat release rate (HRR) for *Photinia fraseri* with (A) size distributions more important in numbers, and (B) size distributions less important in numbers.

particles in number. Finest particles (<71 nm) were the most numerous emitted during the combustion of all fuels. Indeed, for the 25–130 nm range, it is observed that these particles represent 80% to 86% of the particle numbers observed for all fuels.

In order to gain a full understanding of this trend, it is essential to look closely at the evolution of aerosols during the combustion process. A detailed example of this evolution, specifically for the burning of *Photinia fraseri*, is shown in Figure 8. Upon ignition of the shrub and during the subsequent vertical propagation of the fire, we observe the emission of particles with a fine aerodynamic diameter, typically between 25 and 130 nm (Figure 8A). It is particularly notable that these fine particles are the most abundant, and that their concentration closely mirrors the evolution of the HRR (Figure 8A), with maximum aerosol production occurring at the peak of the HRR. As the HRR begins to decrease the number of particles decrease (Figure 8A). When we look in more detail at each stage of the ELPI, the peak production of each aerosol size measured does not occur at the same time. The larger the aerosol size, the later in the combustion process the peak production occurs. For example, the peak between Stage 3 and stage 6 is 64 s compared with 72 s. This observation was noted from Stage 3 to stage 8 for all the different plants. This phenomenon is explained by the widening of the flame as it propagates through the hedge. A similar analysis of the particle size distribution was observed on fires with sheets of different diameters. Mulhland et al.,[39] showed that the volume mean diameter of the primary sphere increases by more than 80% (58 nm vs. 106 nm) as the pan diameter increases from 1 to 3.05 m. During the preheating and pyrolysis phase, organic and inorganic vapors are produced. These inorganic vapors condense in the flue gases and create the fine particles seen on stages 1 and 2. Figure 8B shows the fraction of larger particles and HRR as a function of the time. Prior to the ignition of *Photinia fraseri*, during the preignition phase, we observe the emission of large particles with diameters of 1.65 to 10 µm. These particles are probably tar particles emitted during the preheating phase of the plant.[8] In conclusion, our observations indicate that the highest concentrations of particles are associated with the smaller particles present during the combustion of these fuels. It is also important to note that the number of larger particles remains very low throughout the process (Figure 8B).

The particle number size distribution focuses on the number of particles for each aerosol size class, indicating whether the sample is predominantly composed of small or large particles. This result is of significant importance as it provides information on the quantity of small particles that can penetrate deeply into the human body. There is growing concern within the public health community regarding the contribution of ultrafine particles (UFPs) to human health. Despite their modest mass and size, UFPs dominate in terms of particle numbers in the ambient air. A particular worry is their ability to reach the most distal regions of the lungs (the alveoli) and bypass primary airway defenses.[40] The particle volume distribution, on the other hand, inform us on the volume occupied by each size class of particles, giving an indication of the total mass of the particles and therefore emphasising more on the largest particles than provided by the number size distribution. Figure 9 showed the total mean distribution of number and volume (5 replicates) according the size particles for the all plants. Figure 9A displays the total particle number size distribution produced during the combustion process of each plant. During combustion for the all plants, the distribution size is bimodal and centered on the modes 41 and 71 nm which corresponds to the accumulation mode, for the all plants (Figure 9A). It was observed that the majority of particles had a diameter of less than 1 µm, which is indicative of fine particles, PM_1. Furthermore, it is notable that for all forest fuels, more than 90% of particles were represented by ultrafine particles, $PM_{0.1}$. Figure 9B displays, for the same experiments, the particle size

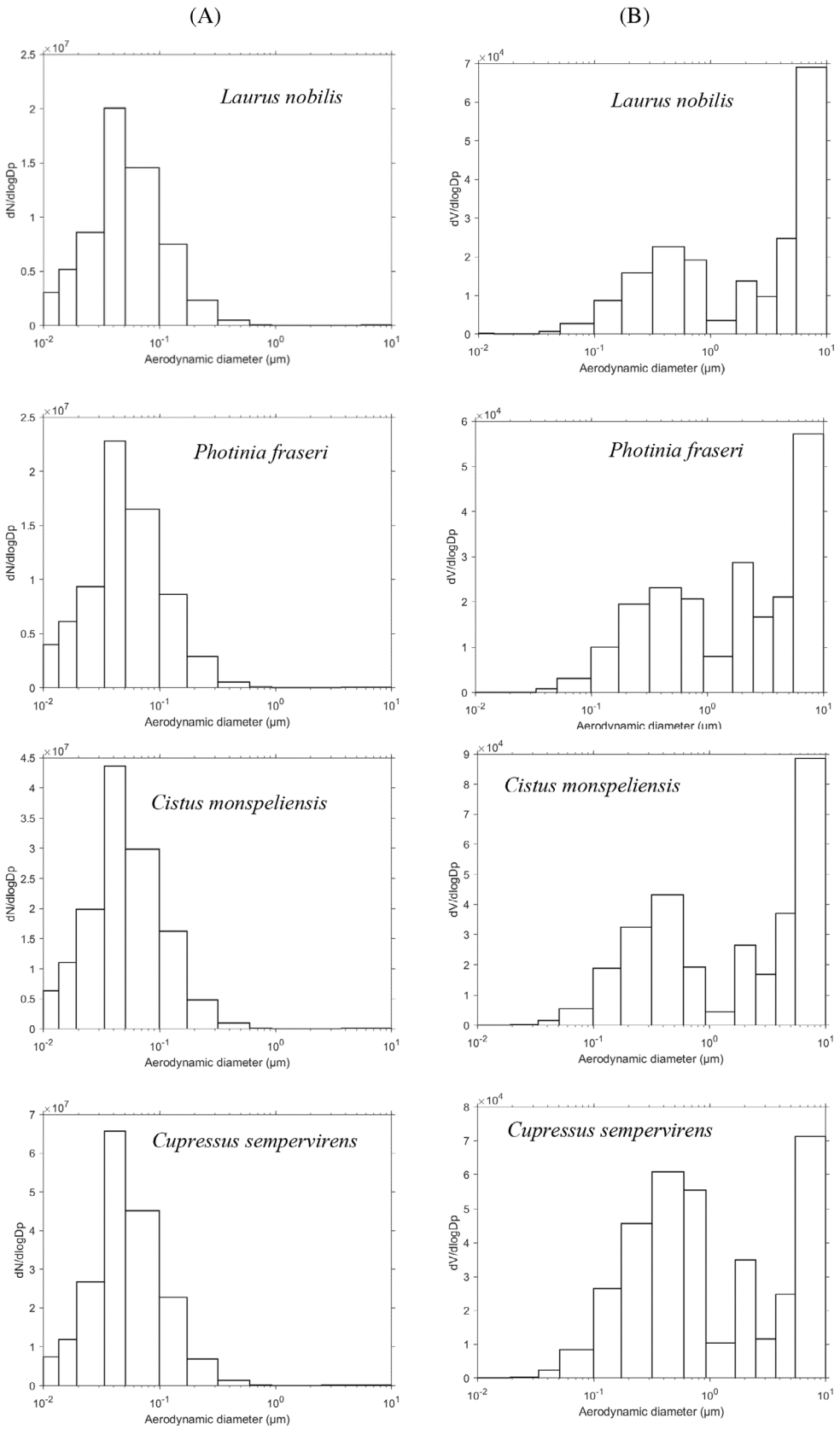


FIGURE 9 Particle size distributions in number (A) and volume (B) emitted during the burning of the four plant species.

distribution in volume as a function of aerodynamic diameter. If the number distribution was centered on the ultrafine and fine particles, however, the analysis of volume distribution gives a different sight of view. For the combustion of the plants, the volume distribution suggests a monomodal distribution excepted the Cupressus plant. This monomodal distribution in volume is centered at 7.369 µm for *Laurus*

TABLE 4 Average emission factors (EF) ($g \cdot kg^{-1}$) emitted during the combustion of the four plants (statistical analysis of compounds according to the fuel, with a > b > c).

Fuel/Compounds	*Laurus nobilis*	*Photinia fraseri*	*Cistus monspeliensis*	*Cupressus sempervirens*
CO_2	1516.24 ± 75.95[b]	1597.72 ± 12.90[b]	1645.65 ± 30.64[a]	1656.60 ± 36.54[a]
CO	150.26 ± 37.47[a]	127.13 ± 6.75[a]	97.35 ± 13.16[b]	77.72 ± 16.39[b]
CH_4	5.81 ± 1.13[a]	4.70 ± 0.37[a]	2.36 ± 0.74[b]	2.65 ± 0.78[b]
NO	12.32 ± 4.84[a]	7.17 ± 0.44[b]	5.32 ± 0.36[c]	6.32 ± 0.27[b]
NO_2	-	-	0.44 ± 0.19[a]	0.42 ± 0.10[a]
NO_x ($NO + NO_2$)	12.32 ± 4.84[a]	7.17 ± 0.44[b]	5.76[c] ± 0.44	6.74[b] ± 0.39
NH_3	0.74 ± 0.19[b]	1.14 ± 0.09[a]	0.31 ± 0.14[c]	0.34 ± 0.03[c]
C_2H_4	2.33 ± 0.64[a]	1.70 ± 0.16[a]	0.86 ± 0.33[b]	1.11 ± 0.34[b]
C_5H_{14}	0.69 ± 0.15[a]	0.68 ± 0.06[a]	0.37 ± 0.12[b]	0.51 ± 0.17[a,b]
CH_2O	0.48 ± 0.07[a]	0.48 ± 0.04[a]	0.23 ± 0.07[b]	0.20 ± 0.08[b]
SO_2	-	-	-	0.86 ± 0.31
Aerosols	1.90 ± 0.77[b]	2.08 ± 0.55[b]	2.12 ± 0.64[b]	4 0.14 ± 0.75[a]
MCE	0.91	0.93	0.94	0.96

Abbreviation: modified combustion efficiency.

nobilis, *Cistus monspeliensis* and *Photinia fraseri*. For and *Cupressus sempervirens*, the distribution of particles volume is superior at 0.1 µm. In conclusion, most of size range of particles distributing on overall volume of particle were mainly composed coarse particle fraction.

3.2.3 | Analysis of smoke compounds

Table 4 presents the compounds identified in the smoke from our experiments as well as their mean EF. The EF contribution of wood wool was subtracted for the all-species contribution and to focus only on the EF of species emitted by the burning of plants. The primary compounds emitted in smoke include CO_2, CO, NO, aerosols, and CH_4, with smaller proportions of C_2H_4, NH_3, C_5H_{14}, CH_2O, SO_2, and NO_2. The EF were averaged across all samples, i.e., five replicates for each species plants. The ANOVA test revealed a statistically significant difference in EF_{CO_2} based on the type of fuel burn (Table 4, ANOVA, $p < 0.05$). The fuels are on influence on EF_{CO_2} the whereas a mean value of were obtained 1516; 1598, 1646; and 1657 $g \cdot kg^{-1}$ for *Laurus nobilis*, *Cistus monspeliensis*, *Photinia fraseri*, and *Cupressus sempervirens* respectively. We note that EF_{CO_2} values are consistent with findings in the literature, which report total EF_{CO_2} ranging between 1538 and 1793 $g \cdot kg^{-1}$.[16,41–44] These last values are derived from laboratory experiments involving different biomass burning scenarios, including savannah and grassland fires, tropical forests, extratropical forests, biofuel combustion, agricultural residues, and Amazonian Forest fires. The emission of various biomass sources such as leaves, woody material, and pine needles from forest fuels have been investigated.[13] We observe the same significant difference with the EF_{CO} (Table 4, ANOVA, $p < 0.05$). Specifically, as *Laurus nobilis* and *Photinia fraseri* burn less efficiently (Table 2), we note that their EF_{CO} is higher for these two species (averaging 127 $g \cdot kg^{-1}$) compared with the other two species (averaging 86 $g \cdot kg^{-1}$). EF_{CO} values reported in the literature show significant variability. Experiments at laboratory scale led to values ranging between 35 and 594 $g \cdot kg^{-1}$.[16,42–48] We observe that the value of EF_{NO} varies significantly depending on the type of fuel burned (Table 4, ANOVA, $p < 0.05$). The highest value of EF_{NO} was observed for the burning of Laurus nobilis. We notice that the higher the percentage of nitrogen (N) present in the virgin plant (see Table 1) the higher the EF_{NO} of the corresponding burning plant. We observe thus that the level of EF_{NO} is influenced by the percentage of nitrogen (%N) present in the fuel. The EF of NOx varies of 5.76 to 12.32 $g \cdot kg^{-1}$, which is stronger the values reported in the literature that range between 1.1 and 4.4 $g \cdot kg^{-1}$.[16,42–44] The emission of NOx is primarily due to NO. The concentration of NOx is contingent upon the nitrogen content of the fuel in question. The values observed in Table 1 align with those expected for NOx concentration and nitrogen elemental analysis. Aerosol production was estimated by using Equation (9) and the He-Ne laser extinction measurement. The decision to calculate the FE with the laser rather than with the Elpi was made for two reasons. Primarily, this approach allows for a comparison of the results with those reported in the literature. Secondly, the exact particle density of the material in question is not known. The composition of the particles includes soot, tar, and ash. Significant differences are observed in the production $EF_{aerosols}$ (Table 4, ANOVA, $p < 0.05$). $EF_{aerosols}$ varies from 4.14 for *Cupressus sempervirens* to 1.9 $g \cdot kg^{-1}$ for *Laurus nobilis*. This difference appears to be linked to the burning behavior. These values are in agreement with the literature, which reports values ranging from 1.5 to 11.9 $g \cdot kg^{-1}$.[11,19,23,25,28–31]

4 | CONCLUSION

In conclusion, the HRR measurements for different plant species revealed significant variations in combustion characteristics. The HRR

increased rapidly after ignition, reaching a peak that varied depending on the species, before declining during the decay phase. Cupressus sempervirens exhibited the highest HRR peak and the longest flame duration, indicating its high combustibility, which is attributed to its greater bulk density and fuel mass. These findings highlight the significant influence of plant species on fire behavior. The experiments identified several key compounds emitted in smoke during the combustion of various plant species, including CO_2, CO, NO, aerosols, and CH_4, with smaller amounts of other gases. EFs were calculated for each compound, with significant differences observed based on the type of fuel burned. In particular, CO EFs was higher for *Laurus nobilis* and *Photinia fraseri* due to less efficient combustion, while the NO EF was closely linked to the nitrogen content of the plant material. Aerosol production also varied significantly among species, reflecting differences in burning behavior. SPR closely follows HRR during combustion, with significant SPR occurring primarily during the flaming stage for all four plant species studied. The highest SPR was observed for *Photinia fraseri*, while Cupressus sempervirens and the other species showed lower SPR values. These findings highlight the influence of plant characteristics and combustion conditions on smoke production, with variations attributed to factors like moisture content and oxygen availability. Our study highlights the complexity of aerosols emitted during the combustion of various fuels, with a predominance of small-size particles (Elpi +). However, a more in-depth analysis reveals a significant contribution of particles larger than 1 µm to the volume distribution, highlighting the importance of understanding the evolution of these aerosols throughout the combustion process. These findings emphasize the need for a holistic approach to fully grasp the characteristics and impacts of aerosols emitted into the WUI.

ORCID

Virginie Tihay-Felicelli https://orcid.org/0000-0001-7723-8808
Toussaint Barboni https://orcid.org/0000-0001-8988-4487

REFERENCES

1. Manzello SL, Blanchi R, Gollner MJ, et al. Summary of workshop large outdoor fires and the built environment. *Fire Saf J*. 2018;100:76-92. doi:10.1016/j.firesaf.2018.07.002
2. Lopes RFR, Modarres M, Rodrigues JPC, Almeida M. Experimental demonstration test of damages in houses caused by wildland-urban interface fires. *Fire Saf J*. 2023;141;103934. doi:10.1016/j.firesaf.2023.103934
3. Ganteaume A, Jappiot M, Lampin C. Assessing the flammability of surface fuels beneath ornamental vegetation in wildland-urban interfaces in Provence (south-eastern France). *Int J Wildland Fire*. 2013;22(3):333-342. doi:10.1071/WF12006
4. Molina-Terrén DM, Xanthopoulos G, Diakakis M, et al. Analysis of forest fire fatalities in southern Europe: Spain, Portugal, Greece and Sardinia (Italy). *Int J Wildland Fire*. 2019;28:85-98. doi:10.1071/WF18004
5. Johnston LM, Flannigan MD. Mapping Canadian wildland fire interface areas. *Int J Wildland Fire*. 2018;27:1-14. doi:10.1071/WF16221
6. Ganteaume A, Barbero R, Jappiot M, Maillé E. Understanding future changes to fires in southern Europe and their impacts on the wildland-urban interface. *J Saf Sci Resil*. 2021;2:20-29. doi:10.1016/j.jnlssr.2021.01.001
7. Radeloff VC, Hammer RB, Stewart SI. Rural and suburban sprawl in the U.S. Midwest from 1940 to 2000 and its relation to Forest fragmentation. *Conserv Biol*. 2005;19:793-805. doi:10.1111/j.1523-1739.2005.00387.x
8. Vacca P, Caballero D, Pastor E, Planas E. WUI fire risk mitigation in Europe: a performance-based design approach at home-owner level. *J Saf Sci Resil*. 2020;1:97-105. doi:10.1016/j.jnlssr.2020.08.001
9. Barboni T, Leonelli L, Santoni P, Tihay-Felicelli V. Aerosols and carbonaceous and nitrogenous compounds emitted during the combustion of dead shrubs according to twigs' diameter and combustion phases. *Fire Saf J*. 2020;113:102988. doi:10.1016/j.firesaf.2020.102988
10. Barboni T, Pellizzaro G, Arca B, et al. Analysis and origins of volatile organic compounds smoke from ligno-cellulosic fuels. *J Anal Appl Pyrolysis*. 2010;89:60-65. doi:10.1016/j.jaap.2010.05.006
11. Barboni T, Cannac M, Pasqualini V, et al. Volatile and semi-volatile organic compounds in smoke exposure of firefighters during prescribed burning in the Mediterranean region. *Int J Wildland Fire*. 2010;19:606-612. doi:10.1071/WF08121
12. Leonelli L, Barboni T, Santoni PA, Quilichini Y, Coppalle A. Characterization of aerosols emissions from the combustion of dead shrub twigs and leaves using a cone calorimeter. *Fire Saf J*. 2017;91:800-810. doi:10.1016/j.firesaf.2017.03.048
13. Santoni P-A, Romagnoli E, Chiaramonti N, Barboni T. Scale effects on the heat release rate, smoke production rate, and species yields for a vegetation bed. *J Fire Sci*. 2015;33(4):290-319. doi:10.1177/0734904115591176
14. Statheropoulos M, Karma S. Complexity and origin of the smoke components as measured near the flame-front of a real forest fire incident: a case study. *J Anal Appl Pyrolysis*. 2007;78:430-437. doi:10.1016/j.jaap.2006.10.011
15. Dokas I, Statheropoulos M, Karma S. Integration of field chemical data in initial risk assessment of forest fire smoke. *Sci Total Environ*. 2007;376:72-85. doi:10.1016/j.scitotenv.2007.01.064
16. Andreae MO, Merlet P. Emission of trace gases and aerosols from biomass burning. *Global Biogeochem Cycles*. 2001;15(4):955-966. doi:10.1029/2000GB001382
17. Yokelson RJ, Burling IR, Urbanski SP, et al. Trace gas and particle emissions from open biomass burning in Mexico. *Atmos Chem Phys*. 2011;11:6787-6808. doi:10.5194/acp-11-6787-2011
18. Hand JL, Malm WC, Laskin A, et al. Optical, physical, and chemical properties of tar balls observed during the Yosemite aerosol characterization study. *J Geophys Res Atmos*. 2005;110:1-14. doi:10.1029/2004JD005728
19. Pósfai M, Simonics R, Li J, Hobbs PV, Buseck PR. Individual aerosol particles from biomass burning in southern Africa: 1 Compositions and Size Distributions of Carbonaceous Particles. *J Geophys Res Atmos*. 2003;108:1-13. doi:10.1029/2002JD002291
20. Naserinejad N, Costanian C, Birot O, et al. Wildland fire, air pollution and cardiovascular health: is it time to focus on the microvasculature as a risk assessment tool? *Front Physiol*. 2023;14:1225195. doi:10.3389/fphys.2023.1225195
21. Jaiswal S, Jalbert I, Schmid K, et al. Smoke and the eyes: a review of the harmful effects of wildfire smoke and air pollution on the ocular surface. *Environ Pollut*. 2022;309:119732. doi:10.1016/j.envpol.2022.119732
22. Fabian TZ, Borgerson JL, Gandhi PD, et al. Characterization of firefighter smoke exposure. *Fire Technol*. 2014;50:993-1019. doi:10.1007/s10694-011-0212-2
23. Tihay V, Santoni PA, Gerandi G, et al. Smoke emissions due to burning of green waste in the Mediterranean area: influence of fuel moisture content and fuel mass. *Atmos Environ*. 2017;159:92-106. doi:10.1016/j.atmosenv.2017.04.002
24. Evtyugina M, Calvo AI, Nunes T, et al. VOC emissions of smouldering combustion from Mediterranean wildfires in central Portugal. *Atmos Environ*. 2013;64:339-348. doi:10.1016/j.atmosenv.2012.10.001

25. Parker WJ. Calculations of the heat release rate by oxygen consumption for various applications. *J Fire Sci*. 1984;2(5):380-395.
26. Huggett C. Estimation of rate of heat release by means of oxygen consumption measurements. *Fire Mater*. 1980;4(2):61-65. doi:10.1002/fam.810040202
27. Santoni P-A, Morandini F, Barboni T. Determination of fireline intensity by oxygen consumption calorimetry. *J Therm Anal Calorim*. 2011;104:1005-1015. doi:10.1007/s10973-010-1256-0
28. Järvinen A, Aitomaa M, Rostedt A, Keskinen J, Yli-Ojanperä J. Calibration of the new electrical low pressure impactor (ELPI+). *J Aerosol Sci*. 2014;69:150-159. doi:10.1016/j.jaerosci.2013.12.006
29. Yli-Ojanperä J, Kannosto J, Marjamäki M, Keskinen J. Improving the nanoparticle resolution of the ELPI. *Aerosol Air Qual Res*. 2010;10:360-366. doi:10.4209/aaqr.2009.10.0060
30. Molina JR, Martín T, Silva FRY, Herrera MÁ. The ignition index based on flammability of vegetation improves planning in the wildland-urban interface: a case study in southern Spain. *Landsc Urban Plan*. 2017;28:85-98. doi:10.1016/j.landurbplan.2016.11.003
31. Lubien D, Shelly J. Defensible space landsaping in the urban/wildland Interface: a compilation of fire performance ratings of residential landsape plants. In: *Forest Product Laboratory Internal Report*. The University of California Forest Products Laboratory. 1997;1-181.
32. Barboni T, Leonelli L, Santoni PA, Tihay-Felicelli V. Influence of particle size on the heat release rate and smoke opacity during the burning of dead cistus leaves and twigs. *J Fire Sci*. 2017;35(4):259-283. doi:10.1177/0734904117709964
33. Vassilev SV, Baxter D, Vassileva CG. An overview of the behaviour of biomass during combustion: part I. Phase-mineral transformations of organic and inorganic matter. *Fuel*. 2013;112:391-449. doi:10.1016/j.fuel.2013.05.043
34. Pagonis D, Selimovic V, Campuzano-Jost P, et al. Impact of biomass burning organic aerosol volatility on smoke concentrations downwind of fires. *Environ Sci Technol*. 2023;57:17011-17021. doi:10.1021/acs.est.3c05017
35. Hodshire AL, Akherati A, Alvarado MJ, et al. Aging effects on biomass burning aerosol mass and composition: a critical review of field and laboratory studies. *Environ Sci Technol*. 2019;53:10007-10022. doi:10.1021/acs.est.9b02588
36. Sipkens TA, Boies A, Corbin JC, Chakrabarty RK, Olfert J, Rogak SN. Overview of methods to characterize the mass, size, and morphology of soot. *J Aerosol Sci*. 2023;173:106211. doi:10.1016/j.jaerosci.2023.106211
37. Tu W-F, Lin JD, Wu YL. An analysis of extinction coefficients of particles and water moisture in the stack after flue gas desulfurization at a coal-fired power plant. *J Air Waste Manage Assoc*. 2011;61(8):815-825. doi:10.3155/1047-3289.61.8.815
38. Srivastava RK, Miller CA, Erickson C, Jambhekar R. Emissions of sulfur trioxide from coal-fired power plants. *J Air Waste Manage Assoc*. 2004;54(6):750-762. doi:10.1080/10473289.2004.10470943
39. Mulholland GW, Liggett W, Koseki H. The effect of pool diameter on the properties of smoke produced by crude oil fires. *Twenty-Sixth Symposium (International) on Combustion/The Combustion Institute*. 1996;1445-1452. doi:10.1016/S0082-0784(96)80365-1
40. Kwon H-S, Ryu MH, Carlsten C. Ultrafine particles: unique physicochemical properties relevant to health and disease. *Exp Mol Med*. 2020;132:22-31. doi:10.1038/s12276-020-0405-1
41. Aurell J, Gullett BK, Tabor D. Emissions from southeastern U.S. grasslands and pine savannas: comparison of aerial and ground field measurements with laboratory burns. *Atmos Environ*. 2015;111:70e178. doi:10.1016/j.atmosenv.2015.03.001
42. Soares Neto TG, Carvalho JA Jr, Cortez EV, et al. Laboratory evaluation of Amazon forest biomass burning emissions. *Atmos Environ*. 2011;45(39):7455-7461. doi:10.1016/j.atmosenv.2011.05.003
43. McMeeking GR, Kreidenweis SM, Baker S, et al. Emissions of trace gases and aerosols during the open combustion of biomass in the laboratory. *J Geophys Res Atmos*. 2009;114(D19):1-20. doi:10.1029/2009JD011836
44. Romagnoli E, Barboni TP, Santoni PA, Chiaramonti N. Quantification of volatile organic compounds in smoke from prescribed burning and comparison with occupational exposure limits. *Nat Hazards Earth Syst Sci*. 2014;5:1049-1057. doi:10.5194/nhess-14-1049-2014
45. Urbanski SP, Hao WM, Baker S. Chemical composition of wildland fire emissions. *Developments in Environmental Science*. Vol 8. Elsevier; 2008;8:79-107.
46. Alves CA, Gonçalves C, Pio CA, et al. Smoke emissions from biomass burning in a Mediterranean shrubland. *Atmos Environ*. 2010;44(25):3024-3033. doi:10.1016/j.atmosenv.2010.05.010
47. Yokelson RJ, Burling IR, Gilman JB, et al. Coupling field and laboratory measurements to estimate the emission factors of identified and unidentified trace gases for prescribed fires. *Atmos Chem Phys*. 2013;13(1):89-116. doi:10.5194/acp-13-89-2013
48. Akagi SK, Yokelson RJ, Wiedinmyer C, et al. Emission factors for open and domestic biomass burning for use in atmospheric models. *Atmos Chem Phys*. 2011;9:4039-4072. doi:10.5194/acp-11-4039-2011

SUPPORTING INFORMATION

Additional supporting information can be found online in the Supporting Information section at the end of this article.

How to cite this article: Martinent B, Luciani C, Tihay-Felicelli V, Renucci F, Santoni P-A, Barboni T. The emission of pollutants from ornamental shrubs during forest fires. *Fire and Materials*. 2025;49(5):585-598. doi:10.1002/fam.3246